Check for updates

Angewandte Chemie International Edition

Angewandte International Edition Chemie

GDCh German Chemical Society

How to cite: *Angew. Chem. Int. Ed.* **2026**, e4623924
doi.org/10.1002/anie.4623924

RESEARCH ARTICLE OPEN ACCESS

Substrate-Controlled Enantiodivergence in Ni-Catalyzed Access to Phosphorylated Oxindoles With Quaternary Stereocenters

Haimeng Zhu[1] | Lewen Wang[1,2] | Shihui Luo[1] | Xinglong Zhang[2] | Jun (Joelle) Wang[1]

[1]Department of Chemistry, Hong Kong Baptist University, Hong Kong, China | [2]Department of Chemistry, The Chinese University of Hong Kong, Hong Kong, China

Correspondence: Xinglong Zhang (xinglong.zhang@cuhk.edu.hk) | Jun (Joelle) Wang (junwang@hkbu.edu.hk)

Received: 29 January 2026 | **Revised:** 19 May 2026 | **Accepted:** 20 May 2026

Keywords: asymmetric synthesis | cascade reactions | heck reactions | homogeneous catalysis | nickel

ABSTRACT

A Ni-catalyzed enantioselective intermolecular Heck-phosphorylation of N-aryl acrylamides with phosphine oxides is developed. This redox-neutral cascade simultaneously forges C—C and C—P bonds, providing direct access to valuable 3,3-disubstituted phosphorylated oxindoles with quaternary stereocenters in good yields and high ee values. Notably, the reaction exhibits a unique substrate-controlled enantiodivergence: simply changing the leaving group (I vs. OTf) on the alkene partner switches the configuration of the product while employing the same enantiomer of the chiral catalyst. The synthetic utility is further demonstrated through product derivatizations. Density functional theory (DFT) calculations reveal that the leaving group dictates the order of migratory insertion versus anion exchange and, crucially, inverts the chiral environment at the enantioselectivity-determining oxidative addition transition state, providing a clear rationale for the observed stereodivergence.

1 | Introduction

Organophosphorus compounds are of significant importance in pharmaceuticals, agrochemistry, organic synthesis, and functional materials [1–7]. Among these, phosphine oxides are particularly valuable motifs; their incorporation into drug candidates is known to enhance biological activity, metabolic stability, and aqueous solubility [8, 9]. Concurrently, chiral 3,3-disubstituted oxindoles constitute a privileged structural motif in numerous pharmaceuticals and natural products [10–13]. Therefore, the development of enantioselective methods for introducing phosphine oxides into oxindole frameworks is highly desirable, offering a direct strategy to access novel, three-dimensional chemical space for drug discovery and diversification.

The asymmetric cascade Heck reaction has emerged as a powerful and atom-economical strategy for constructing heterocycles with challenging all-carbon quaternary stereocenters [14–29]. In particular, enantioselective Heck/cyclization cascades of anilide-tethered alkenes have been developed, enabling C–C bond formations alongside the introduction of diverse functional groups (Scheme 1A) [30–43]. However, methodologies that forge both a C—C and a C—X (X = heteroatom) bond in a single catalytic operation to directly access chiral heteroatom-substituted oxindoles remain very limited (Scheme 1A). Notable progress includes enantioselective intramolecular C—I bond formation. Lautens pioneered the nickel-catalyzed asymmetric intramolecular Heck reaction in 2018, affording 3,3-disubstituted iodooxindoles, albeit with a limited substrate scope [44]. Then in 2020, Lautens and Glorius reported enantioselective

Haimeng Zhu and Lewen Wang contributed equally to this work.

This is an open access article under the terms of the Creative Commons Attribution License, which permits use, distribution and reproduction in any medium, provided the original work is properly cited.
© 2026 The Author(s). *Angewandte Chemie International Edition* published by Wiley-VCH GmbH

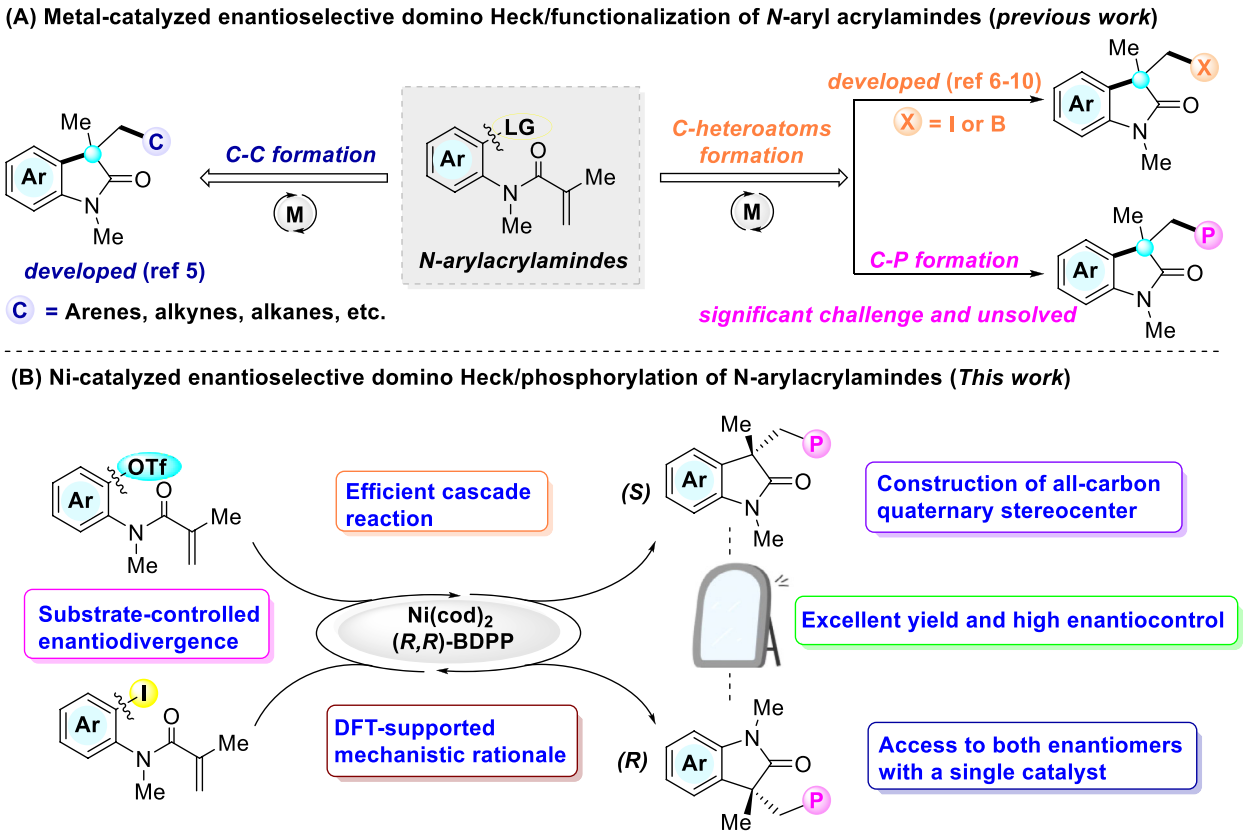

SCHEME 1 | Transition metal catalyzed enantioselective heck/cyclization of tethered alkenes.

nickel-catalyzed carbamoyl iodination by employing a 1,1-disubstituted styrene and KI, thereby expanding the substrate scope [45]. For the C—B bond formation, Lautens [46], Wang [47], and Lu [48] independently developed metal-catalyzed asymmetric borylation/cyclization sequences to access borylated heterocycles. Despite these advances, the direct enantioselective construction of other C–heteroatom bonds, particularly C—P bonds, via a Heck-type cyclization remains an unmet challenge. While racemic synthesis of phosphorylated oxindoles exists [49–55], the competitive coordination of phosphorus species to the metal centers often complicates catalytic cycles and erodes the enantioselectivity.

A distinct and compelling challenge in asymmetric catalysis is achieving enantiodivergence, the ability to access either enantiomer of the products from the same chiral catalyst. This is especially valuable in drug discovery, where enantiomers can exhibit vastly different biological activities [56–64]. In Heck chemistry, such control is rare and typically requires altering the chiral ligand [31]. A strategy to invert enantioselectivity by simply modulating an achiral component of the substrate, while retaining the same chiral catalyst, represents a sophisticated yet undeveloped approach in this field.

Building upon our group's experience in transition metal-catalyzed C—P bond formation [65–78]. and the construction of all-carbon quaternary stereocenters [79], we hypothesized the Ni-catalyzed enantioselective intermolecular Heck-phosphorylation of N-aryl acrylamides with phosphine oxides to merge these domains. While Ni-catalyzed enantioselective reductive Heck reactions typically proceed through a Ni(I)/Ni(III) redox manifold requiring stoichiometric reductants [20, 31–36, 80–82], established Ni(0)-catalyzed asymmetric C—P couplings operate via a Ni(0)/Ni(II) cycle [83–86]. In light of these factors, the Ni(0)-catalyzed redox-neutral pathway could enable an intermolecular Heck phosphorylation cascade without an external reductant (Scheme 1B). This method directly converts N-aryl acrylamides and phosphine oxides into valuable phosphorylated oxindoles bearing quaternary stereocenters in excellent yields and with high enantioselectivity. A particularly powerful feature of this system is its enantiodivergent nature: simply changing the leaving group on the alkene substrate, while employing the same chiral catalyst, provides selective access to either enantiomer of the product.

2 | Results and Discussion

We commenced our study with *o*-iodoaryl anilide (**1a**) and $Ph_2P(O)H$ catalyzed by $Ni(cod)_2$ in DMF (Table 1). An initial ligand screen revealed that the (*R*,*R*)-**BDPP** (**L3**) was the most effective, affording the expected product **3a** with 50% yield in 75% ee (Table 1, entry 3). The enantioselectivity was significantly increased to 85% with an identical yield by employing Li_2CO_3 as the base, while lower ees were obtained by K_2CO_3, Na_2CO_3, or Na_3PO_4 (Table 1, entries 7–9). Further optimization by lowering the reaction temperature and extending the time increased the yield to 90% while maintaining high enantioselectivity (84% ee, entry 10). Notably, switching the substrate to aryl triflate (**2a**) inverted the configuration of the product and provided 80%

15213773, 0, Downloaded from https://onlinelibrary.wiley.com/doi/10.1002/anie.4623924 by The Chinese University of Hong Kong, Wiley Online Library on [08/06/2026]. See the Terms and Conditions (https://onlinelibrary.wiley.com/terms-and-conditions) on Wiley Online Library for rules of use; OA articles are governed by the applicable Creative Commons License

TABLE 1 | Optimization of reaction conditions.[a]

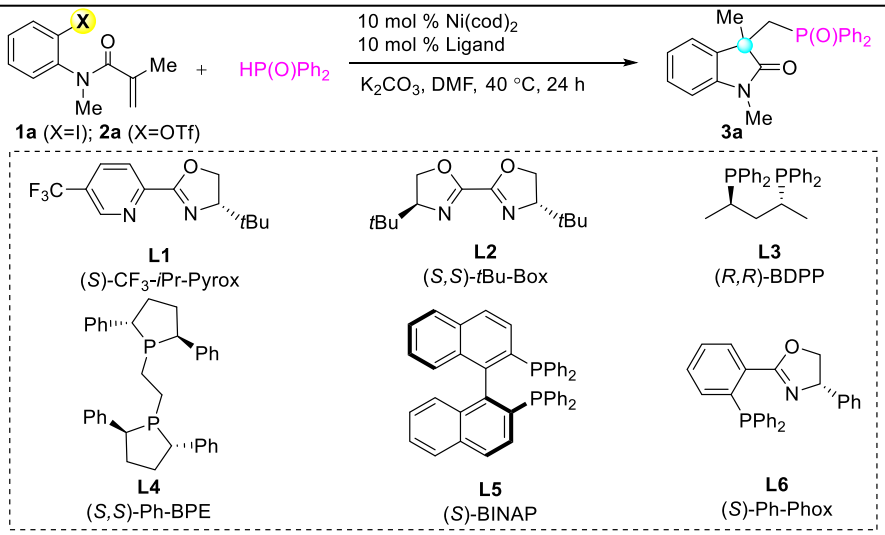

Entry	X	Ligand	Sol.	Base	Yield (%)[b]	*ee* (%)[c]
1	I	L1	DMF	K_2CO_3	—	—
2	I	L2	DMF	K_2CO_3	31	13(*R*)
3	I	L3	DMF	K_2CO_3	50	75(*R*)
4	I	L4	DMF	K_2CO_3	21	60(*R*)
5	I	L5	DMF	K_2CO_3	—	—
6	I	L6	DMF	K_2CO_3	49	20(*R*)
7	I	L3	DMF	Na_2CO_3	55	76(*R*)
8	I	L3	DMF	Na_3PO_4	51	75(*R*)
9	I	L3	DMF	Li_2CO_3	48	85(*R*)
10[d]	**I**	**L3**	**DMF**	**Li_2CO_3**	**94(90)**[f]	**84(*R*)**
11	Br	L3	DMF	K_2CO_3	31	12(*R*)
12	OTs	L3	DMF	K_2CO_3	—	—
13	OTf	L3	DMF	K_2CO_3	49	80(*S*)
14	OTf	L3	DMA	K_2CO_3	39	65(*S*)
15	OTf	L3	CH_3CN	K_2CO_3	95	70(*S*)
16	OTf	L3	DMSO	K_2CO_3	70	78(*S*)
17[e]	OTf	L3	DMSO	K_2CO_3	70	83(*S*)
18[e]	OTf	L3	DMSO	Na_2CO_3	90	82(*S*)
19[e]	**OTf**	**L3**	**DMSO**	**Na_3PO_4**	**97(94)**[f]	**83(*S*)**
20[e]	OTf	L3	DMSO	Et_3N	54	79(*S*)
21[e]	OTf	L3	DMSO	TMG	17	80(*S*)

[a]Conditions: **1a** (0.1 mmol), **2a** (0.15 mmol), $Ni(cod)_2$ (10 mol %), Ligand (10 mol %), Base (2 equiv.), Sol. (1 mL), reaction at 40°C for 24 h.
[b]Yields were determined by ^1H NMR analysis.
[c]Determined by chiral HPLC analysis.
[d]Reaction at 35°C for 6 days.
[e]Reaction at rt for 48 h.
[f]Isolated yield.

ee (entry 13), clearly demonstrating the feasibility of substrate-controlled enantiodivergence.

Based on these results, conditions were further optimized for the reaction of triflate substrate (**2a**) and $Ph_2P(O)H$. A solvent evaluation identified DMSO as optimal, affording **3a** in high yield (entry 16). Lowering the temperature and extending the time to 48 h increased the ee to 83% (entry 17). Subsequent base screening showed that Na_3PO_4 provided an excellent 94% yield while maintaining high enantiocontrol (entries 18–21). Thus, the

15213773, 0, Downloaded from https://onlinelibrary.wiley.com/doi/10.1002/anie.4623924 by The Chinese University of Hong Kong, Wiley Online Library on [08/06/2026]. See the Terms and Conditions (https://onlinelibrary.wiley.com/terms-and-conditions) on Wiley Online Library for rules of use; OA articles are governed by the applicable Creative Commons License

TABLE 2 | Scope of (*S*)-phosphorylated oxindoles.[a]

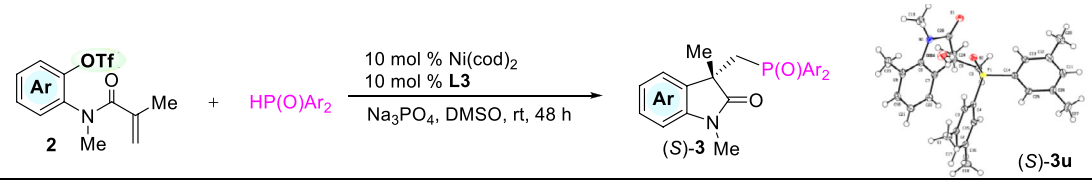

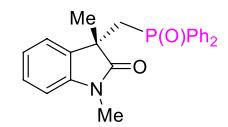

(*S*)-**3a** 94% yield, 83% *ee*

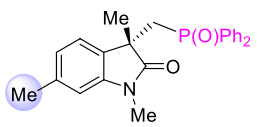

(*S*)-**3b** 97% yield, 84% *ee*

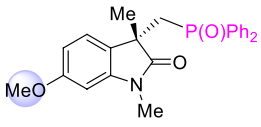

(*S*)-**3c** 98% yield, 90% *ee*

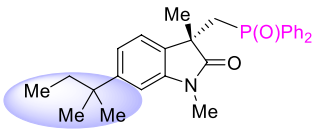

(*S*)-**3d** 99% yield, 87% *ee*

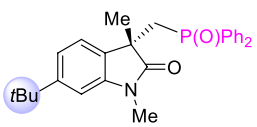

(*S*)-**3e** 95% yield, 88% *ee*

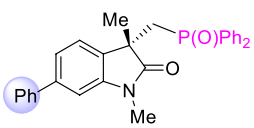

(*S*)-**3f** 92% yield, 73% *ee*

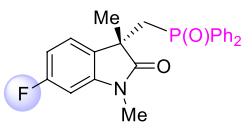

(*S*)-**3g** 99% yield, 70% *ee*

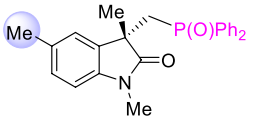

(*S*)-**3h** 98% yield, 89% *ee*

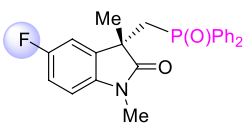

(*S*)-**3i** 99% yield, 70% *ee*

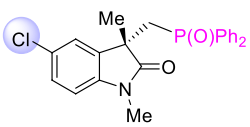

(*S*)-**3j** 99% yield, 70% *ee*

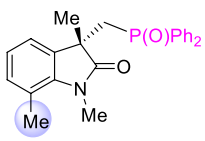

(*S*)-**3k** 99% yield, 94% *ee*[b]

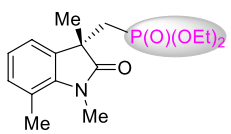

(*S*)-**3l** 78% yield, 84% *ee*[c]

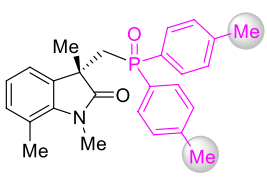

(*S*)-**3m** 95% yield, 94% *ee*[b]

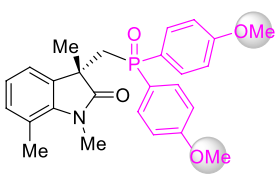

(*S*)-**3n** 98% yield, 92% *ee*[b]

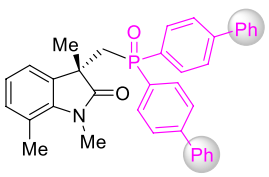

(*S*)-**3o** 99% yield, 94% *ee*[b]

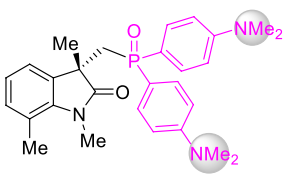

(*S*)-**3p** 86% yield, 90% *ee*[b]

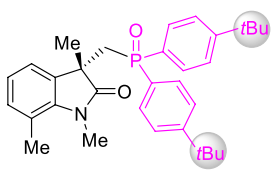

(*S*)-**3q** 98% yield, 93% *ee*[b]

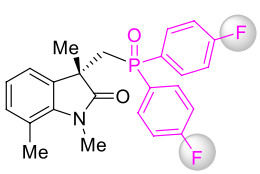

(*S*)-**3r** 70% yield, 94% *ee*[b]

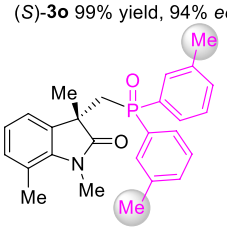

(*S*)-**3s** 93% yield, 95% *ee*[b]

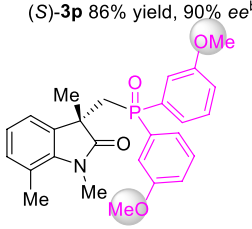

(*S*)-**3t** 99% yield, 93% *ee*[b]

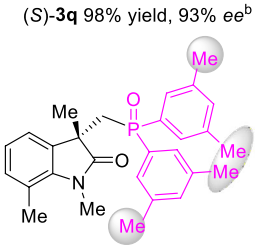

(*S*)-**3u** 99% yield, 92% *ee*[b]

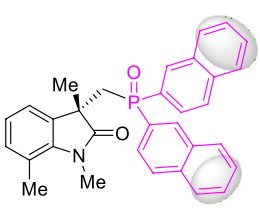

(*S*)-**3v** 99% yield, 93% *ee*[b]

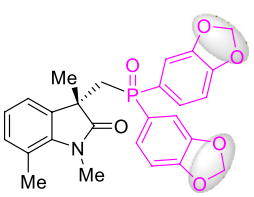

(*S*)-**3w** 99% yield, 93% *ee*[b]

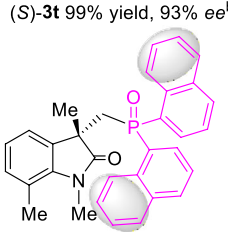

(*S*)-**3x** 70% yield, 94% *ee*[b]

[a]Reaction conditions: **2a** (0.1 mmol), $HP(O)Ar_2$ (0.15 mmol), $Ni(cod)_2$ (10 mol %), **L3** (10 mol %), Na_3PO_4 (2 equiv), DMSO (1 mL), reaction at rt for 48 h under argon; Isolated yields of compounds **3**; ee values are determined by HPLC.[b]Reacted at rt for 4 days.[c]Reacted at 55°C for 5 days.

optimal reaction conditions for aryl iodides were established as $Ni(cod)_2$ (10 mol%), **L3** (10 mol%), and Li_2CO_3 (2 equiv.) in dry DMF at 35°C for 6 days; for aryl triflates, the optimal conditions were $Ni(cod)_2$ (10 mol%), **L3** (10 mol%), and Na_3PO_4 (2 equiv) in dry DMSO at room temperature for 48 h.

With the optimized conditions in hand, the substrate scope was then investigated and is shown in Table 2. A series of aryl triflates with electron-donating groups (e.g., Me, OMe, *t*Amyl and *t*Bu) at the 6-position of the phenyl rings proceeded well, providing products (**3b**-**3e**) in 97%–99% yields with 84–90% ees. Yet, the phenyl group (**3f**) and fluoro group (**3g**) at the 6-position induced a slightly lower ee value (70–73% ee). 5-Methyl substituted acrylamide **1h** with diphenylphosphine oxide, also worked well, affording product **3h** in 98% yield with 89% ee. Aryl triflates bearing electron-withdrawing groups at the 5-position, such as F and

15213773, 0, Downloaded from https://onlinelibrary.wiley.com/doi/10.1002/anie.4623924 by The Chinese University of Hong Kong, Wiley Online Library on [08/06/2026]. See the Terms and Conditions (https://onlinelibrary.wiley.com/terms-and-conditions) on Wiley Online Library for rules of use; OA articles are governed by the applicable Creative Commons License

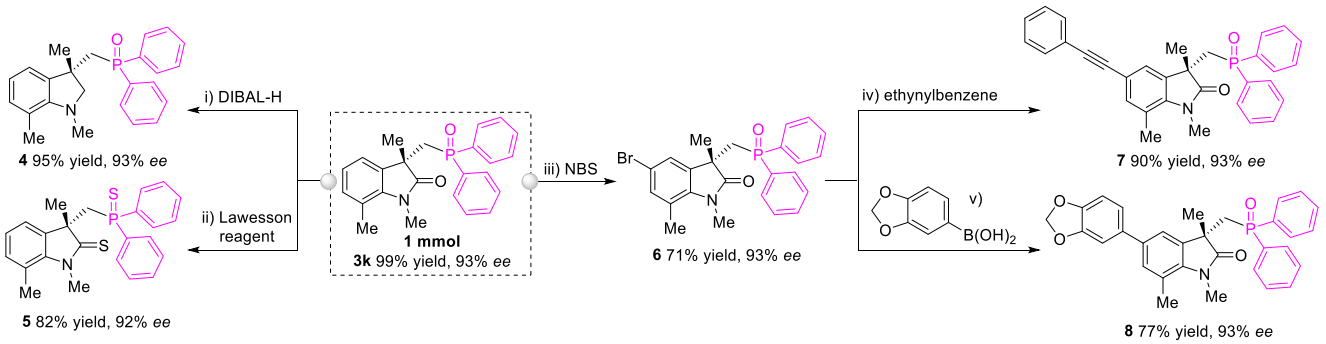

SCHEME 2 | Reaction scale-up and product derivatization: (A) 1mmol-scale synthesis and synthetic transformations (B) enantioselective aldol reaction. Transformations of chiral product **3k**. i) DIBAL-H (8 equiv), toluene, −78°C, 6 h. ii) Lawesson's reagent (1.1 equiv.), toluene, reflux, 12 h. iii) NBS (1.3 equiv.), CH_3CN, rt, 12 h. iv) ethynylbenzene (1.5 equiv), PPh_3(0.2 equiv.), potassium phosphate (1.2 equiv), $Pd(OAc)_2$ (0.05 equiv), DMSO, 100°C, 24 h. v) boronic acid (2 equiv.), $Pd_2(dba)_3$ (0.05 equiv.), PCy_3 (0.1 equiv.), potassium carbonate (2 equiv.), toluene, 100°C, 20 h.

Cl groups, also led to diminished enantioselectivities (99% yield and 79% ee for both **3i** and **3j**). Substrate **1k**, which has a 7-methyl group on the phenyl ring, exhibited excellent enantioselectivity and yield (99% yield, 94% ee). Subsequently, various organophosphorus reagents were examined. Gratifyingly, diethyl phosphite was also compatible and furnished the expected product **3l** with 78% yield and 84% ee. A wide range of diarylphosphine oxides bearing either electron-donating (Me, OMe, Ph, NMe_2, *t*Bu) or an electron-withdrawing group (F) proceeded smoothly, affording chiral phosphorylated oxindoles in good yields with consistently excellent enantioselectivities ranging from 90% to 94% ees (**3m**-**3x**). The absolute configuration of product **3u** was confirmed as (*S*) by single-crystal x-ray structure analysis [87]. Meanwhile, different substituents (-Et, -Ph, and -Bn) were also introduced at the quaternary carbon center, with none affording better results than the methyl group (see Supporting Information for details).

Next, we systematically demonstrated that enantiodivergence could be generalized by simply varying the leaving group from OTf to I while employing the same enantiomer of the BDPP ligand and $Ni(cod)_2$ catalyst (Table 3). Aryl iodides reacted efficiently to give (*R*)-enantiomers of 3,3-disubstituted oxindoles with good yield and high enantioselectivities. Significantly, aryl iodides bearing electron-withdrawing groups on the phenyl ring exhibited remarkably high reactivity and enantioselectivity, but the ee values of (*S*) enantiomers were attenuated (**3g**,**3i,** and **3j**). The reaction scope was further extended to various diarylphosphine oxides, which reliably provided both the (*R*)- and (*S*)-enantiomers (**3ba–3ha**) in high yields and with good enantioselectivity in each series. The absolute configuration of the (*R*)-enantiomer derived from an iodide substrate was unambiguously assigned as (*R*) for product **3j** via single-crystal x-ray diffraction analysis [87]. We also attempted an iodide substrate bearing *β*-substituents and the synthesis of six-membered rings under our standard reaction conditions, yet none furnished satisfactory results (see Supporting Information for details).

The scale-up reaction was performed on the 1 mmol scale, and product **3k** was obtained in 99% yield and 93% ee (Scheme 2A). With compound **3k**, it is feasible to construct a variety of structurally diverse phosphorylated oxindoles. Reduction of **3k** with DIBAL-H yielded enantioenriched oxindole **4** in 95% yield with retention of the enantiopurity. **3k** was readily converted into the thioamide **5** in 82% yield and 92% ee by reaction with Lawesson's reagent. Furthermore, selective bromination at the C5 position of **3k** proceeded smoothly, affording product **6** in 71% yield with 93% ee. The bromination product **6** was further transformed by Sonogashira or Suzuki-Miyaura coupling reaction, respectively, to produce the desired product **7** or **8** without erosion of stereochemical integrity.

To understand the reaction mechanism involving different leaving groups and the factors determining product chirality, density functional theory (DFT) calculations were performed (see Supporting Information for details). The calculated Gibbs energy profiles are shown in Scheme 3. We first determine if the Heck cyclization occurs before or after anion exchange. For the reaction using aryl iodide as the starting material (Scheme 3A), the Heck cyclization transition state after anion exchange (**TS3**) required overcoming a barrier of approximately 30.2 kcal·mol^{-1} (from **INT3′**), whereas the cyclization-first pathway (**TS2**) required only 23.1 kcal·mol^{-1} (from **INT3′**, Scheme 3A). This energy difference indicates that, in the case of aryl iodide substrates, the preferred mechanism proceeds through oxidative addition, followed by Heck cyclization to establish the chiral center, then by anion exchange to replace the leaving group with phosphine oxide, and finally reductive elimination to yield the product.

In contrast, for the reaction employing aryl triflate as the starting material (Scheme 3B), the mechanism sequence is reversed. Here, the reaction favors anion exchange prior to Heck cyclization, as the transition state for migratory insertion prior to anion exchange (**TS2**) exhibits a barrier that is 32.4 kcal·mol^{-1} higher than that of the pathway involving anion exchange followed by migratory insertion (**TS3**). Thus, for aryl triflate, the preferred mechanism proceeds through oxidative addition, followed by anion exchange that replaces the leaving group with a deprotonated phosphine oxide, and then Heck cyclization to establish the chiral center, and finally reductive elimination to afford the product.

For further analysis on enantioselectivity, the enantioselectivity-determining step should be decided first. The Ni(0) oxidative addition process in both reactions is highly exergonic; different isomeric insertions have been fully considered (Figures S2 and S8). A downhill Gibbs energy change is observed from the

15213773, 0, Downloaded from https://onlinelibrary.wiley.com/doi/10.1002/anie.4623924 by The Chinese University of Hong Kong, Wiley Online Library on [08/06/2026]. See the Terms and Conditions (https://onlinelibrary.wiley.com/terms-and-conditions) on Wiley Online Library for rules of use; OA articles are governed by the applicable Creative Commons License

TABLE 3 | Enantiodivergent Synthesis of chiral phosphorylated oxindoles.[a]

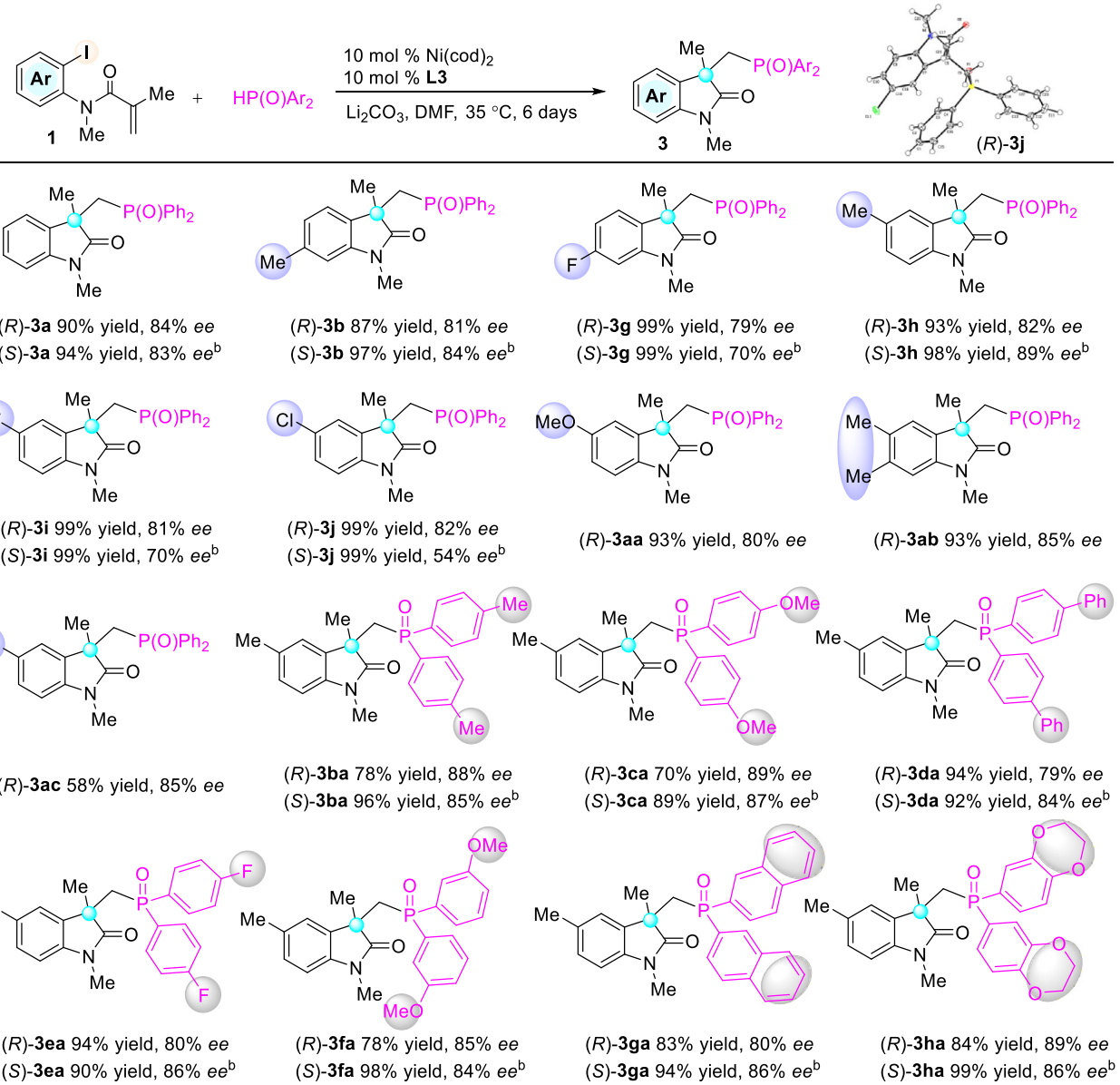

[a]Reaction conditions: **1** (0.1 mmol), $HP(O)Ar_2$ (0.15 mmol), $Ni(cod)_2$ (10 mol%), **L3** (10 mol%), Li_2CO_3 (2 equiv), DMF (1 mL), reaction at 35°C for 6 days under argon; Isolated yields of compounds **3**; ee values are determined by HPLC.[b]**2 (X = OTf) were used instead of 1 (X = I)** (0.1 mmol), $HP(O)Ar_2$ (0.15 mmol), $Ni(cod)_2$ (10 mol %), **L3** (10 mol%), Na_3PO_4 (2 equiv), DMSO (1 mL), reaction at rt for 48 h under argon.

transition state (**TS1**) to the insertion intermediate (**INT2**). For the reaction using aryl iodide, the energy drop from **TS1** to **INT2** is approximately 42.6 kcal·mol^{-1}, whereas for the aryl triflate reaction, this value is about 61.3 kcal·mol^{-1}. These results indicate that the oxidative addition step is irreversible, as reverting from **INT2** to **INT1** via **TS1** will incur very high barriers, as shown in Scheme 3. Furthermore, due to steric hindrance, the isomerization between oxidative addition intermediates (e.g., **INT2a-I** and **INT2c-I**; see Supplementary Information for structural details) is prohibited. The steric repulsion between the phenyl groups of BDPP and the aryl ring of the substrate favors a similar relative orientation of the BDPP–Ni fragment with respect to the substrate in both pathways; in addition, the acrylamide side chain can only approach the reactive site from a single direction to undergo migratory insertion. Consequently, once the oxidative addition proceeds through specific **TS1**, the chirality of the final product is already determined. Therefore, we regard the oxidative addition step as the enantioselectivity-determining step of the reaction; similar conclusions have been arrived in previous research [34].

We next analyzed the molecular origins underlying the enantioselectivity for the experimentally observed single chiral product formation. The DFT-optimized structures, frontier molecular orbitals (HOMO and LUMO), and non-covalent interaction (NCI) plots of the main competing transition states (**TS1a-I** and **TS1c-I** for reaction involving aryl iodide, **TS1a-OTf-O** and **TS1b-OTf-O** for reaction involving aryl triflate) are shown in Figure S3 (aryl iodide) and Figure S9 (aryl triflate), distortion-interaction

15213773, 0, Downloaded from https://onlinelibrary.wiley.com/doi/10.1002/anie.4623924 by The Chinese University of Hong Kong, Wiley Online Library on [08/06/2026]. See the Terms and Conditions (https://onlinelibrary.wiley.com/terms-and-conditions) on Wiley Online Library for rules of use; OA articles are governed by the applicable Creative Commons License

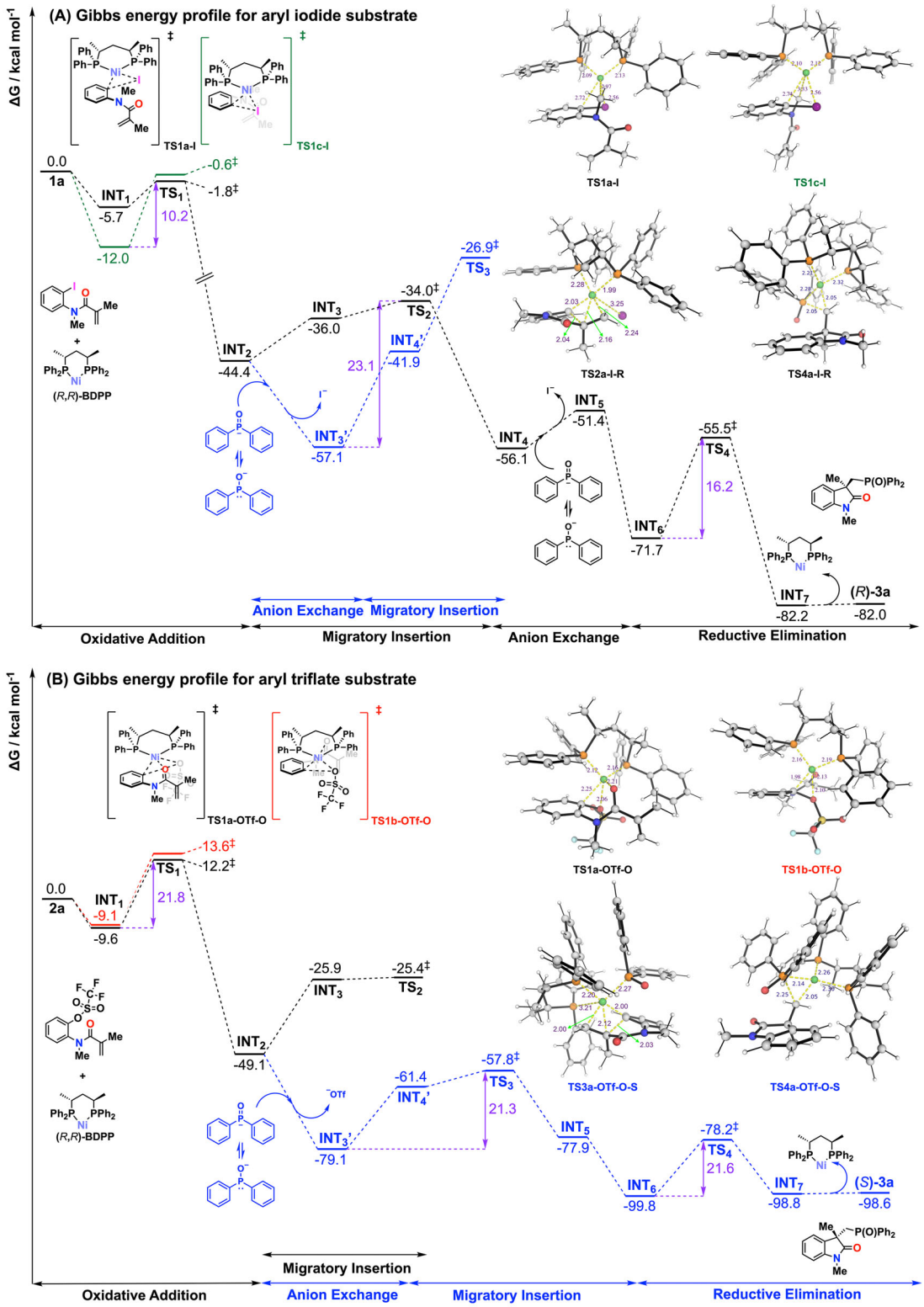

SCHEME 3 | Gibbs energy profiles for model reactions: (A) using aryl iodide and (B) using aryl triflate as starting material.

analysis are shown in Table S1 (aryl iodide) and Table S2 (aryl triflate). For **TS1a-I** and **TS1c-I**, the frontier molecular orbital structures and NCI plots are similar, distortion-interaction analysis reveals that **TS1a-I** has a lower distortion energy (by 1.3 kcal·mol^{-1}), while having a similar interaction energy as **TS1c-I**, therefore **TS1a-I** is favored over **TS1c-I** due to lower steric clashes. For the **TS1a-OTf-O** and **TS1b-OTf-O** pair, **TS1a-OTf-O** exhibits a significantly lower distortion energy in **TS1a-OTf-O** than in **TS1b-OTf-O** by 10.6 kcal·mol^{-1}, despite it having less favorable interaction (by 9.5 kcal·mol^{-1}) such that overall **TS1a-OTf-O** is favored over **TS1b-OTf-O**. In summary, our DFT calculations indicate that the leaving-group identity controls the preferred oxidative-addition geometry. In the aryl iodide pathway, amide O → Ni coordination is disfavored because the gain

15213773, 0, Downloaded from https://onlinelibrary.wiley.com/doi/10.1002/anie.4623924 by The Chinese University of Hong Kong, Wiley Online Library on [08/06/2026]. See the Terms and Conditions (https://onlinelibrary.wiley.com/terms-and-conditions) on Wiley Online Library for rules of use; OA articles are governed by the applicable Creative Commons License

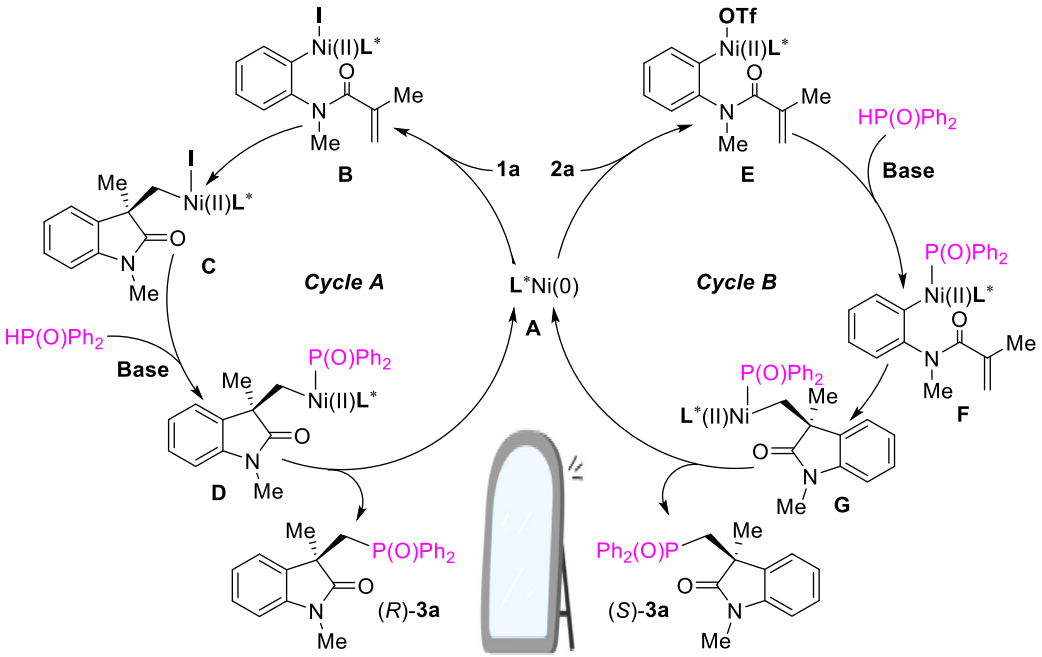

SCHEME 4 | Proposed mechanistic cycles.

in interaction energy cannot compensate for the much higher distortion energy, making the non-coordinated **TS1a-I** lowest in energy (Table S1). By contrast, in the aryl triflate pathway, the oxygen-coordinated **TS1a-OTf-O** is slightly favored (Table S2). Thus, triflate promotes an oxygen-coordinated oxidative-addition mode, whereas iodide does not, and this change in coordination environment, together with the overall balance between steric and electronic influences arising from ligand-catalyst-substrate orientations, leads to the observed enantiodivergence.

Theoretical enantiomeric excess (ee) values for these two model reactions were calculated (see Sections 6.3.4 and 6.4.4 in Supplementary Information). For the reaction using aryl iodide as a starting material at 35°C, by comparing the barriers of **TS1a-I** and **TS1c-I**, the ratio of rate constants for forming the *R*-product and *S*-product can be estimated as $k[R]/k[S] \approx 7.1$, corresponding to an 87.7% proportion of the *R*-enantiomer and a calculated ee of approximately 75%. As for the reaction using aryl triflate as starting material at 25°C, by comparing the barriers of **TS1a-OTf-O** and **TS1b-OTf-O**, the ratio of rate constants for forming the *R*-product and *S*-product can be estimated as $k[R]/k[S] \approx 0.094$, corresponding to an *S*-enantiomer ratio of approximately 91.4% and a calculated ee value of about 83%. The calculated ee values are in good agreement with experimental results.

Based on previous reports [30–43] and our computational results, two distinct catalytic cycles, denoted as cycle A and cycle B, corresponding to the reaction pathways for substrates **1a** and **2a**, respectively, are proposed (Scheme 4). Both cycles start from chiral nickel complex **A**, which is formed from $Ni(cod)_2$ and (*R,R*)-BDPP. As for cycle A, the oxidative addition of C–I bonds to L*Ni(0) gave the Ni(II) specie **B**, followed by an enantioselective 5-exo-trig cyclization to produce intermediate **C**. Then a ligand exchange generates the Ni(II)–P species **D**, accelerated by the base in the presence of the $HP(O)Ph_2$. Further reductive elimination yields the chiral phosphorylated oxindoles (*R*)-**3a** and regenerates reactive L*Ni(0) **A**. Although substrate **2a** in Cycle B similarly first undergoes oxidative addition to form intermediate **E**, DFT calculations reveal that **E** subsequently undergoes a ligand exchange, leading to the formation of intermediate **F**. Following the stereoselective 5-exo-trig intramolecular carbonickelation/migratory insertion, an alkyl-L*Ni(II) intermediate **G** is formed, which can undergo reductive elimination to yield the desired product (*S*)-**3a** and regenerate **A**.

3 | Conclusion

In summary, we have developed an unprecedented Ni-catalyzed enantioselective Heck-phosphorylation cascade between phosphine oxides and anilide-tethered alkenes. This redox-neutral, intermolecular process provides efficient and straightforward access to enantioenriched phosphorylated oxindoles bearing quaternary stereocenters in high yields and excellent enantioselectivities. The methodology features a practical enantiodivergent capability: simply changing the leaving group (I vs. OTf) on the alkene substrate, while using the same chiral catalyst. The synthetic utility was demonstrated through a gram-scale reaction and versatile downstream transformations of the oxindole products. DFT calculations established that the oxidative addition is enantioselectivity-determining and revealed that the divergent stereochemical outcomes originate from leaving-group-controlled chiral environments at this key transition state, providing a clear mechanistic rationale for the observed substrate-driven enantiodivergence.

Author Contributions

Haimeng Zhu: methodology, writing – original draft, conceptualization, and investigation. **Lewen Wang**: writing – original draft, validation, and

15213773, 0, Downloaded from https://onlinelibrary.wiley.com/doi/10.1002/anie.4623924 by The Chinese University of Hong Kong, Wiley Online Library on [08/06/2026]. See the Terms and Conditions (https://onlinelibrary.wiley.com/terms-and-conditions) on Wiley Online Library for rules of use; OA articles are governed by the applicable Creative Commons License

investigation. **Shihui Luo**: methodology and investigation. **Xinglong Zhang**: funding acquisition, supervision, resources, and writing – review and editing. **Jun (Joelle) Wang**: funding acquisition, conceptualization, project administration, writing – review and editing, and supervision.

Acknowledgments

We gratefully acknowledge the Research Grants Council of Hong Kong (SRFS2526-2S02; GRF 12301223), HKBU Faculty Niche Research Areas (IG-FNRA) 2024/25 and HKBU RC-SFCRG/23-24 grant for financial support. X. Z. acknowledges the support of the Vice Chancellor Early Career Professorship Scheme Research Startup Fund (Project Code 4933634) and Research Startup Matching Support (Project Code 5501779) from the Chinese University of Hong Kong (CUHK). The authors acknowledge the facility support from the Advanced Life Sciences and Mass Spectrometry Laboratory (LSMS) of Hong Kong Baptist University. L. W. and X. Z. acknowledge the computational resources at the Central Research Computing Cluster, IT Service Centre at the Chinese University of Hong Kong, partially funded by the Academic Equipment Fund (Project Number 3036253).

Conflicts of Interest

The authors declare no conflicts of interest.

Data Availability Statement

The data that support the findings of this study are available in the supplementary material of this article. DFT optimized structures have been deposited and uploaded to https://zenodo.org/records/17636365 and are freely available.

References

1. M. P. Duffy, W. Delaunay, P. A. Bouit, and M. Hissler, "π-Conjugated Phospholes and Their Incorporation Into Devices: Components With a Great Deal of Potential," *Chemical Society Reviews* 45 (2016): 5296–5310, https://doi.org/10.1039/C6CS00257A.

2. T. K. Warren, R. Jordan, M. K. Lo, et al., "Therapeutic Efficacy of the Small Molecule GS-5734 Against Ebola Virus in Rhesus Monkeys," *Nature* 531 (2016): 381–385, https://doi.org/10.1038/nature17180.

3. G. P. Horsman and D. L. Zechel, "Phosphonate Biochemistry," *Chemical Reviews* 117 (2017): 5704–5783, https://doi.org/10.1021/acs.chemrev.6b00536.

4. H. Ni, W. L. Chan, and Y. Lu, "Phosphine-Catalyzed Asymmetric Organic Reactions," *Chemical Reviews* 118 (2018): 9344–9411, https://doi.org/10.1021/acs.chemrev.8b00261.

5. C. Wang, M. Taki, Y. Sato, et al., "A Photostable Fluorescent Marker for the Superresolution Live Imaging of the Dynamic Structure of the Mitochondrial Cristae," *PNAS* 116 (2019): 15817–15822, https://doi.org/10.1073/pnas.1905924116.

6. T. Imamoto, "P-Stereogenic Phosphorus Ligands in Asymmetric Catalysis," *Chemical Reviews* 124 (2024): 8657–8739, https://doi.org/10.1021/acs.chemrev.3c00875.

7. J.-B. Wang, J. Y. Lv, S. K. Bankar, S.-S. Fang, and M. Shang, "Stereoselective Synthesis of P-Stereogenic Nucleotide Prodrugs and Oligonucleotides," *Chemical Society Reviews* 54 (2025): 9370–9406, https://doi.org/10.1039/D5CS00260E.

8. P. Finkbeiner, J. P. Hehn, and C. Gnamm, "Phosphine Oxides From a Medicinal Chemist's Perspective: Physicochemical and In Vitro Parameters Relevant for Drug Discovery," *Journal of Medicinal Chemistry* 63 (2020): 7081–7107, https://doi.org/10.1021/acs.jmedchem.0c00407.

9. S. Li, T. Zhang, S. J. Zhu, et al., "Optimization of Brigatinib as New Wild-Type Sparing Inhibitors of EGFR T790M/C797S Mutants," *ACS Medicinal Chemistry Letters* 13 (2022): 196–202, https://doi.org/10.1021/acsmedchemlett.1c00555.

10. M. Bandini and A. Eichholzer, "Catalytic Functionalization of Indoles in a New Dimension," *Angewandte Chemie International Edition* 48 (2009): 9608–9644, https://doi.org/10.1002/anie.200901843.

11. I. R. Hardcastle, J. Liu, E. Valeur, et al., "Isoindolinone Inhibitors of the Murine Double Minute 2 (MDM2)-p53 Protein−Protein Interaction: Structure−Activity Studies Leading to Improved Potency," *Journal of Medicinal Chemistry* 54 (2011): 1233–1243, https://doi.org/10.1021/jm1011929.

12. A. Di Mola, L. Palombi, and A. Massa, "Active Methylene Compounds in the Synthesis of 3-Substituted Isobenzofuranones, Isoindolinones and Related Compounds," *Current Organic Chemistry* 16 (2012): 2302–2320, https://doi.org/10.2174/138527212803520254.

13. K. M. McGowan, K. D. Nance, H. P. Cho, et al., "Continued Optimization of the M5 NAM ML375: Discovery of VU6008667, an M5 NAM With High CNS Penetration and a Desired Short Half-Life in Rat for Addiction Studies," *Bioorganic & Medicinal Chemistry Letters* 27 (2017): 1356–1359, https://doi.org/10.1016/j.bmcl.2017.02.020.

14. D. Mc Cartney and P. J. Guiry, "The Asymmetric Heck and Related Reactions," *Chemical Society Reviews* 40 (2011): 5122–5150, https://doi.org/10.1039/C1CS15101K.

15. L.-Q. Lu, J.-R. Chen, and W.-J. Xiao, "Development of Cascade Reactions for the Concise Construction of Diverse Heterocyclic Architectures," *Accounts of Chemical Research* 45 (2012): 1278–1293, https://doi.org/10.1021/ar200338s.

16. H. Cong and G. C. Fu, "Catalytic Enantioselective Cyclization/Cross-Coupling With Alkyl Electrophiles," *Journal of the American Chemical Society* 136 (2014): 3788–3791, https://doi.org/10.1021/ja500706v.

17. Y. Ping, Y. Li, J. Zhu, and W. Kong, "Construction of Quaternary Stereocenters by Palladium-Catalyzed Carbopalladation-Initiated Cascade Reactions," *Angewandte Chemie International Edition* 58 (2019): 1562–1573, https://doi.org/10.1002/anie.201806088.

18. Z. X. Tian, J. B. Qiao, G. L. Xu, et al., "Highly Enantioselective Cross-Electrophile Aryl-Alkenylation of Unactivated Alkenes," *Journal of the American Chemical Society* 141 (2019): 7637–7643, https://doi.org/10.1021/jacs.9b03863.

19. Z. M. Zhang, B. Xu, L. Wu, et al., "Palladium/XuPhos-Catalyzed Enantioselective Carboiodination of Olefin-Tethered Aryl Iodides," *Journal of the American Chemical Society* 141 (2019): 8110–8115, https://doi.org/10.1021/jacs.9b04332.

20. J. He, Y. Xue, B. Han, C. Zhang, Y. Wang, and S. Zhu, "Nickel-Catalyzed Asymmetric Reductive 1,2-Carboamination of Unactivated Alkenes," *Angewandte Chemie International Edition* 59 (2020): 2328–2332, https://doi.org/10.1002/anie.201913743.

21. X. Qi and T. Diao, "Nickel-Catalyzed Dicarbofunctionalization of Alkenes," *ACS Catalysis* 10 (2020): 8542–8556, https://doi.org/10.1021/acscatal.0c02115.

22. A. Whyte, J. Bajohr, R. Arora, A. Torelli, and M. Lautens, "Sequential Pd^0- and Pd^{II}-Catalyzed Cyclizations: Enantioselective Heck and Nucleopalladation Reactions," *Angewandte Chemie International Edition* 60 (2021): 20231–20236, https://doi.org/10.1002/anie.202106518.

23. A. D. Marchese, B. Mirabi, C. E. Johnson, and M. Lautens, "Reversible C—C Bond Formation Using Palladium Catalysis," *Nature Chemistry* 14 (2022): 398–406, https://doi.org/10.1038/s41557-022-00898-0.

24. B. Xu, D. Ji, L. Wu, et al., "Palladium/Xu-Phos-Catalyzed Enantioselective Cascade Heck/Remote C(sp^2)–H Alkylation Reaction," *Chemistry* 8 (2022): 836–849, https://doi.org/10.1016/j.chempr.2021.12.019.

25. Q. Pan, Y. Ping, and W. Kong, "Nickel-Catalyzed Ligand-Controlled Selective Reductive Cyclization/Cross-Couplings," *Accounts of Chemical Research* 56 (2023): 515–535, https://doi.org/10.1021/acs.accounts.2c00771.

26. L. Zou, Y. Gao, Q. Zhang, et al., "Recent Progress in Asymmetric Domino Intramolecular Cycliza-tion/Cascade Reactions of Substituted Olefins," *Chemistry: An Asian Journal* 18 (2023): e202300617, https://doi.org/10.1002/asia.202300617.

15213773, 0, Downloaded from https://onlinelibrary.wiley.com/doi/10.1002/anie.4623924 by The Chinese University of Hong Kong, Wiley Online Library on [08/06/2026]. See the Terms and Conditions (https://onlinelibrary.wiley.com/terms-and-conditions) on Wiley Online Library for rules of use; OA articles are governed by the applicable Creative Commons License

27. A. D. Marchese, E. M. Larin, B. Mirabi, and M. Lautens, "Metal-Catalyzed Approaches Toward the Oxindole Core," *Accounts of Chemical Research* 53 (2020): 1605–1619, https://doi.org/10.1021/acs.accounts.0c00297.

28. Y. J. Jang, E. M. Larin, and M. Lautens, "Rhodium-Catalyzed Enantioselective Reductive Arylation: Convenient Access to 3,3-Disubstituted Oxindoles," *Angewandte Chemie International Edition* 56 (2017): 11927–11930, https://doi.org/10.1002/anie.201704922.

29. W. Zu, H. Wu, J. Huo, et al., "Enantioselective Incorporation of Amine Fragments Onto Quaternary Carbons via Metallaphotoredox Catalysis," *Angewandte Chemie International Edition* 64 (2025): e202513309.

30. J. Yao, C. Zhao, L. Shao, X. Huo, and X. Wang, "Synergistic Asymmetric Diarylation of Tethered Alkenes via C—H Functionalization of Simple (Hetero)Arenes," *Science China Chemistry* 67 (2024): 2710–2718, https://doi.org/10.1007/s11426-024-2059-y.

31. Q. Pan, K. Wang, W. Xu, et al., "Ligand-Controlled, Nickel-Catalyzed Stereodivergent Construction of 1,3-Nonadjacent Stereocenters," *Journal of the American Chemical Society* 146 (2024): 15453–15463, https://doi.org/10.1021/jacs.4c03745.

32. C. Zhao, Z. Ge, J. Hu, H. Tian, and X. Wang, "Enantioselective Reductive Aryl-Benzylation of Alkenes by a Nickel-Titanium Bimetallic System," *Cell Reports Physical Science* 4 (2023): 101474, https://doi.org/10.1016/j.xcrp.2023.101474.

33. G. Wang, C. Shen, X. Ren, and K. Dong, "Ni-Catalyzed Enantioselective Reductive Arylcyanation/Cyclization of *N*-(2-iodo-aryl) Acrylamide," *Chemical Communications* 58 (2022): 1135–1138, https://doi.org/10.1039/D1CC04996H.

34. X. W. Chen, J. P. Yue, K. Wang, et al., "Nickel-Catalyzed Asymmetric Reductive Carbo-Carboxylation of Alkenes With CO_2," *Angewandte Chemie International Edition* 60 (2021): 14068–14075, https://doi.org/10.1002/anie.202102769.

35. T. Ma, Y. Chen, Y. Li, Y. Ping, and W. Kong, "Nickel-Catalyzed Enantioselective Reductive Aryl Fluoroalkenylation of Alkenes," *ACS Catalysis* 9 (2019): 9127–9133, https://doi.org/10.1021/acscatal.9b03172.

36. K. Wang, Z. Ding, Z. Zhou, and W. Kong, "Ni-Catalyzed Enantioselective Reductive Diarylation of Activated Alkenes by Domino Cyclization/Cross-Coupling," *Journal of the American Chemical Society* 140 (2018): 12364–12368, https://doi.org/10.1021/jacs.8b08190.

37. D. Zhang, Y. Xiong, Y. Guo, L. Zhang, Z. Wang, and K. Ding, "Palladium-Catalyzed Enantioselective Intramolecular Heck Carbonylation Reactions: Asymmetric Synthesis of 2-Oxindole Ynones and Carboxylic Acids," *Chemistry: A European Journal* 28 (2022): e202103670, https://doi.org/10.1002/chem.202103670.

38. M. Chen, X. Wang, P. Yang, X. Kou, Z. H. Ren, and Z. H. Guan, "Palladium-Catalyzed Enantioselective Heck Carbonylation With a Monodentate Phosphoramidite Ligand: Asymmetric Synthesis of (+)-Physostigmine, (+)-Physovenine, and (+)-Folicanthine," *Angewandte Chemie International Edition* 59 (2020): 12199–12205, https://doi.org/10.1002/anie.202003288.

39. X. Bai, C. Wu, S. Ge, and Y. Lu, "Pd/Cu-Catalyzed Enantioselective Sequential Heck/Sonogashira Coupling: Asymmetric Synthesis of Oxindoles Containing Trifluoromethylated Quaternary Stereogenic Centers," *Angewandte Chemie International Edition* 59 (2020): 2764–2768, https://doi.org/10.1002/anie.201913148.

40. S. Tong, A. Limouni, Q. Wang, M. X. Wang, and J. Zhu, "Catalytic Enantioselective Double Carbopalladation/C—H Functionalization With Statistical Amplification of Product Enantiopurity: A Convertible Linker Approach," *Angewandte Chemie International Edition* 56 (2017): 14192–14196, https://doi.org/10.1002/anie.201709133.

41. W. Kong, Q. Wang, and J. Zhu, "Synthesis of Diversely Functionalized Oxindoles Enabled by Migratory Insertion of Isocyanide to a Transient σ-Alkylpalladium(II) Complex," *Angewandte Chemie International Edition* 55 (2016): 9714–9718, https://doi.org/10.1002/anie.201603950.

42. W. You and M. K. Brown, "Catalytic Enantioselective Diarylation of Alkenes," *Journal of the American Chemical Society* 137 (2015): 14578–14581, https://doi.org/10.1021/jacs.5b10176.

43. W. Kong, Q. Wang, and J. Zhu, "Palladium-Catalyzed Enantioselective Domino Heck/Intermolecular C—H Bond Functionalization: Development and Application to the Synthesis of (+)-Esermethole," *Journal of the American Chemical Society* 137 (2015): 16028–16031, https://doi.org/10.1021/jacs.5b11625.

44. H. Yoon, A. D. Marchese, and M. Lautens, "Carboiodination Catalyzed by Nickel," *Journal of the American Chemical Society* 140 (2018): 10950–10954, https://doi.org/10.1021/jacs.8b06966.

45. A. D. Marchese, M. Wollenburg, B. Mirabi, et al., "Nickel-Catalyzed Enantioselective Carbamoyl Iodination: A Surrogate for Carbamoyl Iodides," *ACS Catalysis* 10 (2020): 4780–4785, https://doi.org/10.1021/acscatal.0c00841.

46. A. Whyte, K. I. Burton, J. Zhang, and M. Lautens, "Enantioselective Intramolecular Copper-Catalyzed Borylacylation," *Angewandte Chemie International Edition* 57 (2018): 13927–13930, https://doi.org/10.1002/anie.201808460.

47. J. Chen, J.-H. Li, Y.-P. Zhu, and Q.-A. Wang, "Copper-Catalyzed Enantioselective Arylboronation of Activated Alkenes Leading to Chiral 3,3′-Disubstituted Oxindoles," *Organic Chemistry Frontiers* 8 (2021): 2532–2536, https://doi.org/10.1039/D1QO00186H.

48. X. Bai, W. Zheng, S. Ge, and Y. Lu, "Enantioselective Palladium-Catalyzed Arylborylation/Cyclization of Alkenes to Access Boryl-Functionalized Heterocyclic Compounds Containing Quaternary Stereogenic Centers," *Organic Letters* 24 (2022): 3080–3085, https://doi.org/10.1021/acs.orglett.2c01082.

49. Y.-J. Zhang, X.-S. Wang, J. Cao, and L.-W. Xu, "A General Platform for Phosphorylation Reactions Enabled by Photoinduced Palladium Catalysis," *Green Chemistry* 26 (2024): 8360–8366, https://doi.org/10.1039/D4GC00918E.

50. X. Zhou, J. Wang, Y. Shen, D. Ma, Y. Zhao, and J. Wu, "Cp_2Fe-Mediated Electrochemical Synthesis of Phosphorylated Oxindoles and Indolo[2,1-*a*]isoquinolin-6(5*H*)-Ones," *Journal of Organic Chemistry* 88 (2023): 17521–17526, https://doi.org/10.1021/acs.joc.3c02017.

51. Y. Y. Pan, X. W. Zhu, L. Shi, G. Jiang, and X. X. Wu, "Palladium-Catalyzed Heck Cyclization With P(O)H Compounds to Construct Phosphinonyl-Azaindoline and -Azaoxindole Derivatives," *Journal of Organic Chemistry* 88 (2023): 9843–9852, https://doi.org/10.1021/acs.joc.3c00521.

52. C. Chen, W. Sun, Y. Yan, et al., "Palladium-Catalyzed Phosphoryl-Carbamoylation of Alkenes: Construction of Nonbenzylic C(sp^3)—P(O)R_2 Bonds via C(sp^3)—Pd(II)—P(O)R_2 Reductive Elimination," *Advanced Synthesis & Catalysis* 362 (2020): 2970–2975, https://doi.org/10.1002/adsc.202000337.

53. K. Ramesh and G. Satyanarayana, "Microwave-Assisted Domino Heck Cyclization and Phosphorylation: Synthesis of Phosphorus Containing Heterocycles," *European Journal of Organic Chemistry* 2019 (2019): 3856–3866, https://doi.org/10.1002/ejoc.201900510.

54. G. Lu, X. Huangfu, Z. A. Wu, G. Tang, and Y. Zhao, "Palladium-Catalyzed Domino Heck/Phosphorylation Towards 3,3-Disubstituted Phosphinonyloxindoles," *Advanced Synthesis & Catalysis* 361 (2019): 4961–4965, https://doi.org/10.1002/adsc.201901100.

55. Y. M. Li, M. Sun, H. L. Wang, Q. P. Tian, and S. D. Yang, "Direct Annulations Toward Phosphorylated Oxindoles: Silver-Catalyzed Carbon-Phosphorus Functionalization of Alkenes," *Angewandte Chemie International Edition* 52 (2013): 3972–3976, https://doi.org/10.1002/anie.201209475.

56. I. P. Beletskaya, C. Najera, and M. Yus, "Stereodivergent Catalysis," *Chemical Reviews* 118 (2018): 5080–5200, https://doi.org/10.1021/acs.chemrev.7b00561.

15213773, 0, Downloaded from https://onlinelibrary.wiley.com/doi/10.1002/anie.4623924 by The Chinese University of Hong Kong, Wiley Online Library on [08/06/2026]. See the Terms and Conditions (https://onlinelibrary.wiley.com/terms-and-conditions) on Wiley Online Library for rules of use; OA articles are governed by the applicable Creative Commons License

57. B. Kim, H. Lee, I. Song, and S. Y. Lee, "Diastereodivergence in Catalytic Asymmetric Conjugate Addition of Carbon Nucleophiles," *Chemical Society Reviews* 54 (2025): 715–741, https://doi.org/10.1039/D4CS00485J.

58. S. Krautwald and E. M. Carreira, "Stereodivergence in Asymmetric Catalysis," *Journal of the American Chemical Society* 139 (2017): 5627–5639, https://doi.org/10.1021/jacs.6b13340.

59. W. L. Cui, L. Zhang, C. Liu, et al., "Reagent-Regulated Organocatalytic Enantiodivergent Synthesis of Chiral Sulfinimidate Esters," *Journal of the American Chemical Society* 147 (2025): 19986–19995, https://doi.org/10.1021/jacs.5c05035.

60. Z. Yang, M. Pu, L. Yang, et al., "Metal-Controlled Enantiodivergent Tandem Rearrangement to Synthesize 2*H*-Azirines," *Angewandte Chemie International Edition* 64 (2025): e202505725, https://doi.org/10.1002/anie.202505725.

61. H. Y. Kim, J. Y. Li, S. Kim, and K. Oh, "Stereodivergency in Catalytic Asymmetric Conjugate Addition Reactions of Glycine (Ket)imines," *Journal of the American Chemical Society* 133 (2011): 20750–20753, https://doi.org/10.1021/ja2100356.

62. T. T. Gao, W. W. Zhang, X. Sun, H. X. Lu, and B. J. Li, "Stereodivergent Synthesis Through Catalytic Asymmetric Reversed Hydroboration," *Journal of the American Chemical Society* 141 (2019): 4670–4677, https://doi.org/10.1021/jacs.8b13520.

63. D. A. Khrakovsky, C. Tao, M. W. Johnson, R. T. Thornbury, S. L. Shevick, and F. D. Toste, "Enantioselective, Stereodivergent Hydroazidation and Hydroamination of Allenes Catalyzed by Acyclic Diaminocarbene (ADC) Gold(I) Complexes," *Angewandte Chemie International Edition* 55 (2016): 6079–6083, https://doi.org/10.1002/anie.201601550.

64. Q. Yang, Z. Wang, C. H. H. Hor, H. Xiao, Z. Bian, and J. Wang, "Asymmetric Synthesis of Flavanols via Cu-Catalyzed Kinetic Resolution of Chromenes and Their Anti-Inflammatory Activity," *Science Advances* 8 (2022): eabm9603, https://doi.org/10.1126/sciadv.abm9603.

65. Z. Yang, X. Gu, L.-B. Han, and J. Wang, "Modular Assembly of Axially Chiral QUINAP Derivatives via Nickel-Catalyzed Enantioselective C—P Cross-Coupling," *ACS Catalysis* 15 (2025): 8268–8273, https://doi.org/10.1021/acscatal.5c01663.

66. S. Luo, X. Yuan, J. Cheng, Z. Yang, Z. Huang, and J. Wang, "Enantioselective Zn-Catalyzed Hydrophosphinylation of Nitrones: An Efficient Approach for Constructing Chiral α-Hydroxyamino-Phosphine Oxides," *Chemical Science* 16 (2025): 7051–7056, https://doi.org/10.1039/D5SC01453K.

67. Y. Jiang, K. W. Cheng, Z. Yang, and J. Wang, "Pd-Catalyzed Enantioselective and Regioselective Asymmetric Hydrophosphorylation and Hydrophosphinylation of Enynes," *Chinese Chemical Letters* 36 (2025): 110231–110237, https://doi.org/10.1016/j.cclet.2024.110231.

68. X.-D. Gu, K. Y. Ngai, W. Wang, B. Li, and J. Wang, "Ni-Catalyzed Propargylic Substitution Reaction: A General and Versatile Tool to Assemble Axially Chiral Phosphorus-Containing Allenes," *Chem Catalysis* 4 (2024): 100903–100916, https://doi.org/10.1016/j.checat.2024.100903.

69. J. Zhou, L. Meng, S. Lin, B. Cai, and J. Wang, "Palladium-Catalyzed Enantio- and Regioselective Ring-Opening Hydrophosphinylation of Methylenecyclopropanes," *Angewandte Chemie International Edition* 62 (2023): e202303727, https://doi.org/10.1002/anie.202303727.

70. Q. Yang, J. Zhou, and J. Wang, "Enantioselective Copper-Catalyzed Hydrophosphination of Alkenyl Isoquinolines," *Chemical Science* 14 (2023): 4413–4417, https://doi.org/10.1039/D2SC06950D.

71. B. Cai, Y. Cui, J. Zhou, et al., "Asymmetric Hydrophosphinylation of Alkynes: Facile Access to Axially Chiral Styrene-Phosphines," *Angewandte Chemie International Edition* 62 (2023): e202215820, https://doi.org/10.1002/anie.202215820.

72. Y. Zhang, Y. Jiang, M. Li, Z. Huang, and J. Wang, "Palladium-Catalyzed Diastereo- and Enantioselective Desymmetric Hydrophosphination of Cyclopropenes," *Chem Catalysis* 2 (2022): 3163–3173, https://doi.org/10.1016/j.checat.2022.08.008.

73. H. Zhu, K. Takeda, Z. Yang, R. Takita, and J. Wang, "Pd-Catalyzed Asymmetric P–C Cross-Coupling to Access *ortho*-NH2 or -OH aryl P-Chiral Phosphine Oxides," *Cell Reports Physical Science* 6 (2025): 102798, https://doi.org/10.1016/j.xcrp.2025.102798.

74. Z. Yang and J. Wang, "Enantioselective Palladium-Catalyzed Hydrophosphinylation of Allenes With Phosphine Oxides: Access to Chiral Allylic Phosphine Oxides," *Angewandte Chemie International Edition* 60 (2021): 27288–27292, https://doi.org/10.1002/anie.202112285.

75. Z. Yang, X. Gu, L. B. Han, and J. Wang, "Palladium-Catalyzed Asymmetric Hydrophosphorylation of Alkynes: Facile Access to P-Stereogenic Phosphinates," *Chemical Science* 11 (2020): 7451–7455, https://doi.org/10.1039/D0SC01049A.

76. Z. Lu, H. Zhang, Z. Yang, N. Ding, L. Meng, and J. Wang, "Asymmetric Hydrophosphination of Heterobicyclic Alkenes: Facile Access to Phosphine Ligands for Asymmetric Catalysis," *ACS Catalysis* 9 (2019): 1457–1463, https://doi.org/10.1021/acscatal.8b04787.

77. J. Zhou, S. Tao, X. Zhang, and J. Wang, "Additive-Controlled Regioswitching in Ni-Catalyzed Enantioselective Hydrophosphination of Unactivated Alkenes," *Journal of the American Chemical Society* 148, no. 3 (2026): 3481–3490, https://doi.org/10.1021/jacs.5c19022.

78. J.-T. Cheng, X. Yuan, Z. Yang, K. Liu, and J. Wang, "Construction of Tetrasubstituted α-Amino- and α-Alkoxy Phosphine Oxides via Pd-Catalyzed Regio- and Enantioselective Hydrophosphinylation of Dienes," *Angewandte Chemie International Edition* 64 (2025): e202519578, https://doi.org/10.1002/anie.202519578.

79. X. Gu, K. Liu, L. Yang, C. Xie, M. Li, and J. Wang, "Nickel-Catalyzed Enantioselective α-Heteroarylation of Ketones via C—F Bond Activation to Construct All-Carbon Quaternary Stereocenters," *Chemical Science* 13 (2022): 12498–12502, https://doi.org/10.1039/D2SC03409C.

80. Z. Chen and Z. Shen, "Nickel-Catalyzed Asymmetric Reductive Arylcyanation of Alkenes With Acetonitrile as the Cyano Source," *Organic Chemistry Frontiers* 10 (2023): 745–751, https://doi.org/10.1039/D2QO01727J.

81. S. Ni, F. L. Vaillant, A. Mateos-Calbet, R. Martin, and J. Cornella, "Ni-Catalyzed Oxygen Transfer From N_2O Onto sp^3-Hybridized Carbons," *Journal of the American Chemical Society* 144 (2022): 18223–18228, https://doi.org/10.1021/jacs.2c06227.

82. Y. Ping, K. Wang, Q. Pan, et al., "Ni-Catalyzed Regio- and Enantioselective Domino Reductive Cyclization: One-Pot Synthesis of 2,3-Fused Cyclopentannulated Indolines," *ACS Catalysis* 9 (2019): 7335–7342, https://doi.org/10.1021/acscatal.9b02081.

83. X. Zhang, S.-Q. Wang, and S.-D. Yang, "Nickel-Catalyzed Kinetic Resolution to Achieve P-Chiral Phosphine Oxides and sec-Phosphine Oxides," *Science China Chemistry* 66 (2023): 2569–2575, https://doi.org/10.1007/s11426-023-1678-1.

84. Q.-W. Zhang, R.-R. Cui, and Q. Zhang, "Nickel-Catalyzed Asymmetric Arylation of H-Phosphinates," *Synlett* 34 (2023): 1819–1823, https://doi.org/10.1055/s-0042-1751456.

85. C. Wang, X. Hu, C. Xu, et al.,"Synthesis of P-Stereogenic Phosphine Oxides via Nickel-Catalyzed Asymmetric Cross-Coupling of Secondary Phosphine Oxides With Alkenyl and Aryl Bromides", *Angewandte Chemie International Edition* 62 (2023): e20e2300011.

86. R. Cui, Y. Wang, L. Yuwen, et al., "Ni-Catalyzed Asymmetric C—P Cross-Coupling Reaction for the Synthesis of Chiral Heterocyclic Phosphine Oxides," *Organic Letters* 25 (2023): 6139–6142, https://doi.org/10.1021/acs.orglett.3c02216.

87. Deposition Number 2498377 (for **3u**) and 2492738 (for **3j**) contain the supplementary crystallographic data for this paper. Copies of the data can be obtained free of charge via, https://www.ccdc.cam.ac.uk/structures/.

Supporting Information

Additional supporting information can be found online in the Supporting Information section.

Supporting File: anie73012-sup-0001-SuppMat.docx.

15213773, 0, Downloaded from https://onlinelibrary.wiley.com/doi/10.1002/anie.202623924 by The Chinese University of Hong Kong, Wiley Online Library on [08/06/2026]. See the Terms and Conditions (https://onlinelibrary.wiley.com/terms-and-conditions) on Wiley Online Library for rules of use; OA articles are governed by the applicable Creative Commons License